Article

Structure

Structural Basis of Formation of the Microtubule Minus-End-Regulating CAMSAP-Katanin Complex

Graphical Abstract

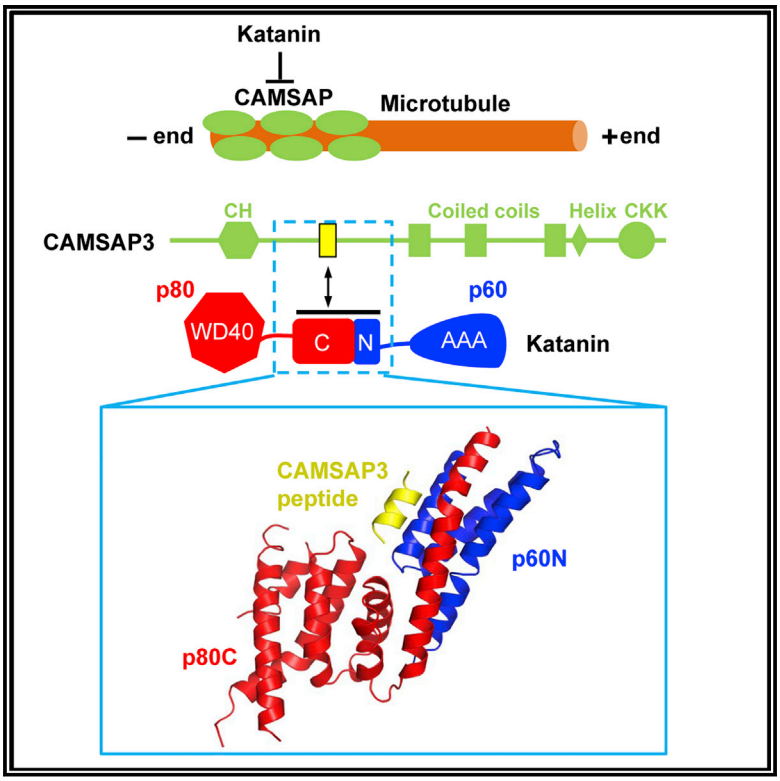

Highlights

- A short helical motif of CAMSAP3 binds to the katanin p60/p80 heterodimer interface
- Complex formation between CAMSAP3 and p60/p80 is driven by hydrophobic interactions
- The microtubule-minus-end regulators CAMSAP and ASPM bind to the same site on katanin
- A point mutation in p80 affects the length of CAMSAP-protected microtubule minus ends

Authors

Kai Jiang, Lenka Faltova, Shasha Hua, ..., Richard A. Kammerer, Michel O. Steinmetz, Anna Akhmanova

Correspondence

richard.kammerer@psi.ch (R.A.K.), michel.steinmetz@psi.ch (M.O.S.), a.akhmanova@uu.nl (A.A.)

In Brief

CAMSAPs are proteins that control the organization of microtubule networks by decorating and stabilizing microtubule minus ends. Jiang et al. characterize the binding mode between CAMSAPs and the microtubule-severing enzyme katanin. Disruption of the CAMSAP-katanin interaction demonstrates that katanin is a negative regulator of microtubule minus-end stabilization by CAMSAPs.

Jiang et al., 2018, Structure *26*, 375–382
March 6, 2018
https://doi.org/10.1016/j.str.2017.12.017

CellPress

Structure
Article

Structural Basis of Formation of the Microtubule Minus-End-Regulating CAMSAP-Katanin Complex

Kai Jiang,[1,5] Lenka Faltova,[2,5] Shasha Hua,[1] Guido Capitani,[2] Andrea E. Prota,[2] Christiane Landgraf,[3] Rudolf Volkmer,[3] Richard A. Kammerer,[2,*] Michel O. Steinmetz,[2,4,*] and Anna Akhmanova[1,6,*]
[1]Cell Biology, Department of Biology, Faculty of Science, Utrecht University, Padualaan 8, 3584 Utrecht, the Netherlands
[2]Laboratory of Biomolecular Research, Division of Biology and Chemistry, Paul Scherrer Institut, 5232 Villigen, Switzerland
[3]Institut für Medizinische Immunologie, Charité-Universitätsmedizin Berlin, Leibniz-Institut für Molekulare Pharmakologie, 10117 Berlin, Germany
[4]University of Basel, Biozentrum, 4056 Basel, Switzerland
[5]These authors contributed equally
[6]Lead Contact
*Correspondence: richard.kammerer@psi.ch (R.A.K.), michel.steinmetz@psi.ch (M.O.S.), a.akhmanova@uu.nl (A.A.)
https://doi.org/10.1016/j.str.2017.12.017

SUMMARY

CAMSAP/Patronin family members regulate the organization and stability of microtubule minus ends in various systems ranging from mitotic spindles to differentiated epithelial cells and neurons. Mammalian CAMSAP2 and CAMSAP3 bind to growing microtubule minus ends, where they form stretches of stabilized microtubule lattice. The microtubule-severing ATPase katanin interacts with CAMSAPs and limits the length of CAMSAP-decorated microtubule stretches. Here, by using biochemical, biophysical, and structural approaches, we reveal that a short helical motif conserved in CAMSAP2 and CAMSAP3 binds to the heterodimer formed by the N- and C-terminal domains of katanin subunits p60 and p80, respectively. The identified CAMSAP-katanin binding mode is supported by mutational analysis and genome-editing experiments. It is strikingly similar to the one seen in the ASPM-katanin complex, which is responsible for microtubule minus-end regulation in mitotic spindles. Our work provides a general molecular mechanism for the cooperation of katanin with major microtubule minus-end regulators.

INTRODUCTION

Microtubules are dynamic cytoskeletal polymers that drive chromosome separation during cell division and form tracks for intracellular transport. Microtubules are intrinsically asymmetric, with a dynamic plus end and a more stable minus end (Akhmanova and Steinmetz, 2015). The organization of minus ends plays a major role in defining the architecture of microtubule arrays (Akhmanova and Hoogenraad, 2015; Dammermann et al., 2003). In interphase animal cells, microtubules can adopt a radial arrangement due to their attachment to the centrosome. However, most differentiated cells have a non-centrosomal microtubule organization, and even in cells with a radial microtubule network, a significant proportion of microtubules is not attached to the centrosome but is tethered to the Golgi apparatus or is distributed in the cytoplasm (Akhmanova and Hoogenraad, 2015; Dammermann et al., 2003). Recently, members of the CAMSAP/Patronin family emerged as major regulators responsible for the stability of non-centrosomal microtubules (Goodwin and Vale, 2010; Jiang et al., 2014; Meng et al., 2008). In mammalian cells, this family is represented by three homologs, CAMSAP1, CAMSAP2, and CAMSAP3 (also known as Nezha or Marshalin) (Baines et al., 2009; Meng et al., 2008; Zheng et al., 2013). While CAMSAP1 dynamically tracks microtubule minus ends, CAMSAP2 and CAMSAP3 are stably deposited on the elongating microtubule minus ends and form stretches of stabilized microtubule lattice (Jiang et al., 2014). These stretches prevent microtubule disassembly from both ends and can serve as "seeds" for microtubule outgrowth (Jiang et al., 2014).

Since the deposition of CAMSAP2 and CAMSAP3 on microtubule minus ends strongly stabilizes the microtubule lattice, an important question is how such lattices are disassembled. Previous work has shown that CAMSAP2 and CAMSAP3 interact with the microtubule-severing-protein katanin, which is required for limiting the length of CAMSAP2/3 bound microtubule minus-end stretches (Jiang et al., 2014). Katanin consists of the catalytic subunit p60, which belongs to the AAA family of ATPases, and an accessory subunit p80 (Hartman et al., 1998; McNally and Vale, 1993; Roll-Mecak and McNally, 2010). Our recent work revealed that the N-terminal part of p60 (p60N) and the C-terminal part of p80 (p80C) form a heterodimeric, helical protein module that can bind, decorate, bend, and break dynamic microtubule ends (Jiang et al., 2017; Rezabkova et al., 2017). Interestingly, the p60N/p80C heterodimer binds to a short linear polypeptide repeat of the spindle-pole-associated protein ASPM (abnormal spindle-like microcephaly associated) (Jiang et al., 2017). Similar to CAMSAPs, ASPM is an autonomous minus-end binding protein (Jiang et al., 2017); however, while CAMSAP2 and CAMSAP3 act in interphase cells and are

removed from microtubules during cell division due to phosphorylation (Jiang et al., 2014; Syred et al., 2013), ASPM only binds to microtubules in mitosis. The ASPM-katanin complex controls the dynamics of microtubule minus ends at the spindle poles, and the loss of ASPM and katanin leads to a strong reduction of astral microtubules and abnormal spindle positioning. These observations provide clues as to why mutations in genes encoding ASPM and katanin p80 are associated with microcephaly, a congenital genetic syndrome whereby patients are born with a small head and brain due to abnormalities in proliferation of neuronal progenitors (Bond et al., 2002; Hu et al., 2014; Mishra-Gorur et al., 2014; Mochida and Walsh, 2001). Several microcephaly-associated mutations affect the structure of the p60N/p80C heterodimer as well as its binding to ASPM, supporting the importance of the ASPM-katanin interaction and its role in controlling microtubule minus ends in mitosis (Jiang et al., 2017)

Here, we set out to get a deeper insight into the katanin-containing complexes that regulate microtubule minus ends in interphase. We investigated the binding mode between CAMSAP3 and katanin by biochemical, biophysical, and structural approaches and found that it involves the interface formed between the two subunits of the katanin p60N/p80C heterodimer, which is very similar to the ASPM binding site. Biophysical analyses confirmed competitive binding of CAMSAP3 and ASPM to katanin p60N/p80C. The CAMSAP-katanin binding mode identified is strongly supported by mutational analysis, including a mutation of a single critical residue in the endogenous p80 subunit in human cells. Our work thus reveals a remarkable similarity in the way katanin cooperates with two unrelated microtubule regulators, ASPM and CAMSAP, which are responsible for controlling microtubule minus-end dynamics in mammalian mitosis and interphase, respectively.

RESULTS

A Short Peptide Segment of CAMSAP3 Binds to the Katanin Heterodimer

CAMSAPs contain a C-terminal CKK domain responsible for minus-end recognition, several predicted coiled-coil regions, and an N-terminal calponin homology (CH) domain, the function of which is unknown (Figure 1A) (Atherton et al., 2017; Jiang et al., 2014). Our previous work showed that a region located between the CH domain and the first coiled coil of CAMSAP2 is responsible for the interaction with katanin (Jiang et al., 2014). We have now mapped the CAMSAP-katanin interaction in more detail using CAMSAP3 and found that a short polypeptide fragment (CAMSAP3p1, residues 456–470) is necessary and sufficient for pulling down endogenous katanin subunits from HEK293T cell extracts (Figures 1A and 1B). This region is well conserved in CAMSAP2 and CAMSAP3 from different vertebrate species (Figure 1C), and secondary structure predictions using JPred (Drozdetskiy et al., 2015) suggest that it might adopt a helical conformation.

To map the sequence requirements for the interaction from the katanin side, we performed pull-down assays using the CAMSAP3p1 fragment fused to the C terminus of GST (GST-CAMSAP3p1) as bait and lysates of HEK293T cells expressing GFP-tagged katanin p60 and p80 subunits. A strong interaction was only observed when p60 and p80 were co-expressed, but not when either subunit was expressed individually (Figure 1D). Since our recent study showed that the N terminus of p60 (p60N) and the C terminus of p80 (p80C) form a tight heterodimer (Jiang et al., 2017; Rezabkova et al., 2017), we tested whether the p60N/p80C complex is sufficient for the binding to GST-CAMSAP3p1 and found that it was indeed the case (Figures 1A and 1E).

Since the CAMSAP3 fragment containing sequences C-terminal to CAMSAP3p1 (CAMSAP3-C1) bound to katanin much better than the N-terminal fragment (CAMSAP3-N2, Figure 1B), we next investigated whether a longer CAMSAP3 peptide, residues 456–520, would have a higher affinity for the p60N/p80C complex. However, we found that the longer peptide actually interacted less well with p60N/p80C (Figure S1). This result suggests that the unfolded region located C-terminally of CAMSAP3p1 somehow reduces the affinity of the peptide for binding. The higher affinity of CAMSAP3-FL and CAMSAP3-C1 compared with CAMSAP3-N2 for katanin (Figure 1B) is thus likely caused by the coiled-coil regions that enhance the avidity of CAMSAP3 for the p60/p80 complex. We concluded that a short CAMSAP3 peptide segment interacts with the complex formed between p60N and p80C.

Structural Basis of the CAMSAP3-Katanin Interaction

To elucidate the molecular details of the CAMSAP-katanin interaction, we reconstituted a minimal tripartite 1:1:1 stoichiometric complex composed of p60N, p80C, and a short CAMSAP3 peptide, and characterized it by biophysical methods and X-ray crystallography. First, we performed sedimentation velocity analytical ultracentrifugation (SV AUC) experiments with a fluorescein isothiocyanate (FITC)-labeled CAMSAP3 peptide (FITC-CAMSAP3p1). When the peptide was combined with p60N or p80C alone, we observed no FITC-specific peak in the continuous sedimentation coefficient, c(S), distribution profile, indicating that no binding of the peptide to individual katanin subunits occurred (Figure 2A). However, upon addition of the p60N/p80C complex, a peak at 2.5 ± 0.1 S was obtained, indicating complex formation (Figure 2A). The presence of both p60N and p80C is thus a prerequisite for FITC-CAMSAP3p1 binding, in agreement with our pull-down data (Figure 1E). Moreover, by performing the same experiments with different concentrations of p60N/p80C (Figures S2A and S2B), we found that the FITC-CAMSAP3p1 peptide binds to the katanin heterodimer with an apparent dissociation constant, K_D, of 2.4 ± 0.2 μM.

In order to obtain crystals of the tripartite p60N/p80C/CAMSAP3 complex, we screened CAMSAP3 peptides of different lengths. Well-diffracting crystals were obtained with a 10-amino acid-long CAMSAP3 peptide (residues 461–470, denoted CAMSAP3p2). The structure was solved by molecular replacement in space group $P2_1$ using the p60N/p80C chains of the p60N/p80C/ASPMp complex as a search model (Jiang et al., 2017), and refined to 1.7 Å resolution with two copies of a 1:1:1 p60N/p80C/CAMSAP3p2 complex in the asymmetric unit Table 1. The electron density map around the CAMSAP3p2 peptide is shown in Figures S3A and S3B. In agreement with our previous data (Jiang et al., 2017; Rezabkova et al., 2017), p60N forms an antiparallel three-helix bundle that interacts with the seven-helix bundle formed by p80C (Figure 2C). The CAMSAP3p2 peptide was found to bind at the interface between the p60N and

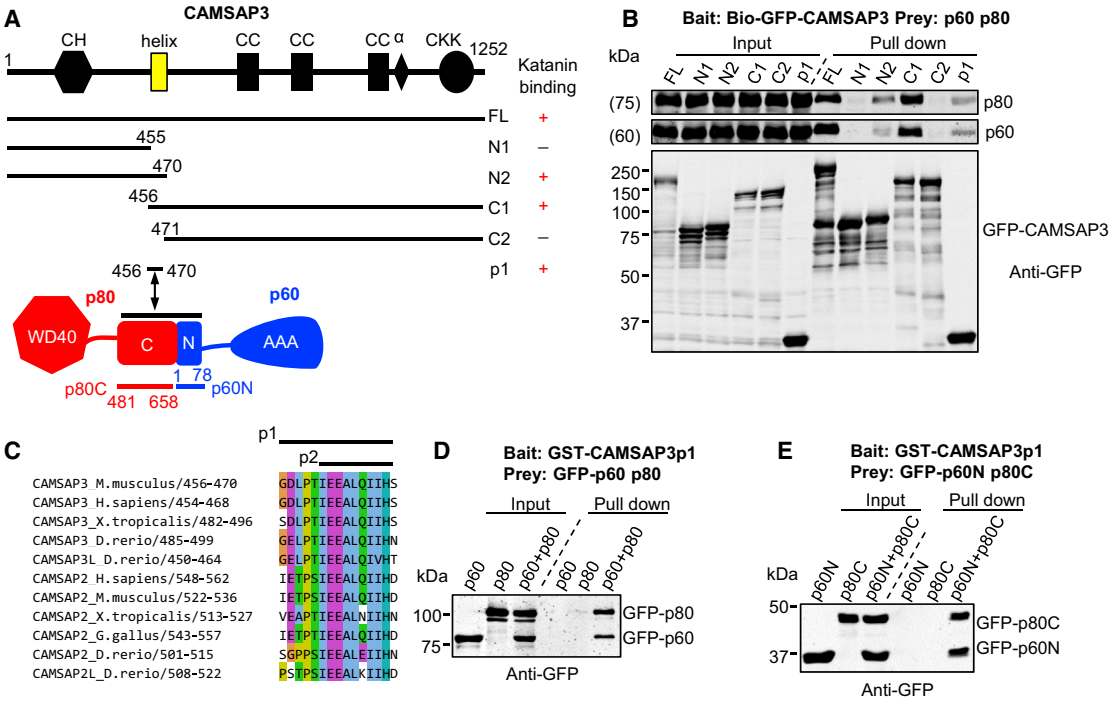

Figure 1. The Interaction between CAMSAP2/3 and Katanin Is Mediated by a Conserved Peptide Segment of CAMSAP2/3 and the p60N/p80C Heterodimer

(A) Schematic representation of the domain organization of CAMSAP3, p60, and p80 and summary of the interaction between CAMSAP3 and katanin. α, alpha helix; AAA, ATPases associated with diverse cellular activities domain; C, C terminus of p80; CC, coiled coil; CH, calponin homology domain; CKK, common to CAMSAP1, KIAA1078, and KIAA1543; helix, katanin-interacting helix; N, N terminus of p60; WD40, WD40 repeat domain. The numbering of the protein sequence is based on mouse proteins.

(B) Streptavidin pull-down assay with lysates of HEK293T cells expressing full-length CAMSAP3 or its fragments, which were fused to GFP and the biotinylation tag.

(C) Alignment of katanin-binding helices of CAMSAP2/3 from several vertebrate species. The positions of the two peptides used in this study, CAMSAP3p1 and CAMSAP3p2, are indicated. Clustal W coloring scheme is used: hydrophobic amino acids, blue; negatively charged, magenta; aromatic, cyan; polar, green; yellow, prolines, orange, glycines.

(D) GST-CAMSAP3p1 pull-down assay with lysates of HEK293T cells expressing individual GFP-tagged subunits of katanin or the p60/p80 heterodimer.

(E) GST-CAMSAP3p1 pull-down assay with lysates of HEK293T cells expressing individual fragments of katanin or the p60N/p80C heterodimer.

See also Figure S1.

p80C domains, as predicted by our biophysical data (Figure 2A). Although CAMSAP3p2 is disordered in the unbound state, as shown by circular dichroism spectroscopy (Figure S2C), the peptide adopts a helical conformation when complexed with p60N/p80C (Figure 2C). Molecular recognition between p60N/p80C and CAMSAP3p2 is mediated by hydrophobic interactions: Residues L18 and L19 of p60N and M501 and Y574 of p80C establish hydrophobic contacts with I461, L465, I467, and I468 of CAMSAP3p2 (Figure 2D).

To confirm the importance of L18 and L19 of p60N and M501 and Y574 of p80C for the interaction with CAMSAP3, we individually mutated these residues to alanine. Notably, these mutations had no effect on the formation and stability of the p60/p80 heterodimer (Figures S2D–S2F; Jiang et al., 2017). However, all these mutations strongly inhibited the binding between GST-CAMSAP3p1 and p60/p80 in pull-down experiments, confirming their importance for tripartite complex formation (Figure 2B). The microcephaly-associated p80 S538L mutation also disrupted the binding of GST-CAMSAP3p1 (Figure 2B), suggesting that the loss of CAMSAP3 association with katanin might contribute to the microcephaly phenotype. Notably, residue S538 of the p80 subunit is 4.8 Å away from the side chain of I461 of CAMSAP3p2 in the p60N/p80C/CAMSAP3p2 complex structure and is therefore not directly involved in binding. However, mutation of S538 to leucine destabilizes the katanin structure (Figure S2F), and we assume that such a destabilization leads to a reduction in affinity for CAMSAP3p2.

To investigate the importance of single CAMSAP3 residues for the interaction with p60N/p80C, we employed synthetic peptide arrays on cellulose membrane supports (SPOT). We generated an array of 20-residue peptides (residues 455–474, denoted CAMSAPp3) encompassing the sequence of the CAMSAPp2 peptide used for crystallization. The peptide array shown in Figure 2E represents a complete amino acid substitution analysis, in which each residue of CAMSAPp3 was substituted individually by all naturally occurring amino acids. The array was subsequently probed for p60N/p80C binding, which is reflected by black spots of variable intensities. Visual inspection of the SPOT array results confirmed that all the hydrophobic residues of CAMSAPp2 are crucial for p60N/p80C interaction and tolerate

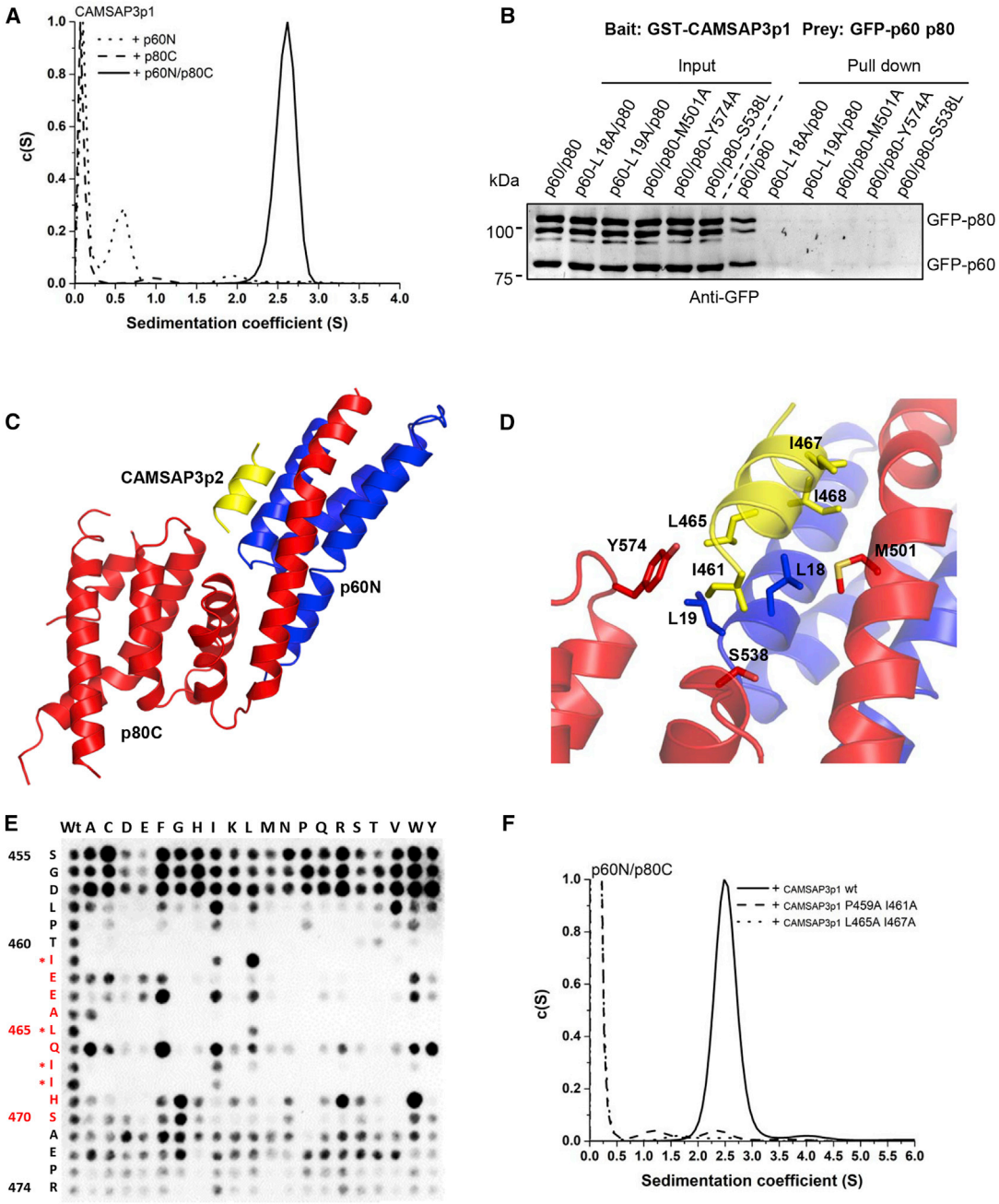

Figure 2. Biophysical and Structural Characterization of the CAMSAP-Katanin Interaction

(A) Continuous sedimentation coefficient (c(S)) distribution profiles showing that p60N/p80C complex formation is a prerequisite for FITC-CAMSAP3p1 peptide binding. No interaction was observed between FITC-CAMSAP3p1 and the p60N or p80C subunits alone. SV AUC profiles were recorded with 490 nm excitation, which allows specific detection of the FITC-labeled CAMSAP3p1 peptide.

(B) GST pull-down assay with GST-CAMSAP3p1 and lysates of HEK293T cells expressing GFP-tagged wild-type (WT) or mutant p60/p80 heterodimers.

(C) Cartoon representation of the crystal structure of the tripartite p60N/p80C/CAMSAP3p2 complex. p60N, p80C, and the CAMSAP3p2 peptide are shown in blue, red, and yellow, respectively.

(D) Close-up view of the CAMSAP3 binding site. Interacting residues are shown in stick representation.

(E) SPOT analysis of the CAMSAPp3 peptide. Black spots indicate interactions between p60N/p80C and membrane-bound CAMSAPp3 variants. Each spot corresponds to a variant in which one residue of the CAMSAPp3 sequence (given on the left) was replaced by one of the 20 gene-encoded amino acids (shown at the top). The residues of the CAMSAP3p2 (AA 461–470) used in the crystal structure are highlighted in red; asterisks denote hydrophobic residues identified in the crystal structure as important for the interaction with p60N/p80C.

(F) c(S) distribution profiles showing that the indicated mutations in FITC-CAMSAP3p1 peptide abolished the interaction with p60N/p80C. The SV AUC profiles were recorded at 490 nm.

See also Figures S2 and S3.

Table 1. X-Ray Data Collection and Refinement Statistics

	p60N/p80C/CAMSAP3p2
Data Collection	
Space group	$P2_1$
Cell dimensions	
a, *b*, *c* (Å)	36.3, 79.1, 99.1
α, β, γ (°)	90, 95.0, 90
Resolution (Å)[a]	50.0–1.7 (1.79–1.7)
No. of reflections	59,910 (7963)
R_{meas} (%)	8.0 (113.4)
$I/\sigma I$	17.8 (1.6)
$CC_{1/2}$	99.9 (64.4)
Completeness (%)	97.5 (91.0)
Redundancy	11.5 (7.3)
Refinement	
Resolution (Å)	41.9–1.7 (1.79–1.7)
No. of unique reflections	59,903
R_{work}/R_{free} (%)	19.1/23.2 (30.8/35.3)
Average B factors (Å2)	
Complex	43.5
Solvent	43.9
Wilson B factor	26.1
Root-mean-square deviation from ideality	
Bond length (Å)	0.009
Bond angles (°)	0.897
Ramachandran statistics[b]	
Favored regions (%)	99.2
Allowed regions (%)	0.8
Outliers (%)	0

[a]Highest-resolution shell is shown in parentheses.
[b]As defined by MolProbity (Davis et al., 2004).

almost no substitutions. In addition to the hydrophobic residues that are seen in the p60N/p80C/CAMSAP3p2 complex structure, P459 and T460 of CAMSAP3 also appeared to be important for binding, as hardly any substitutions were tolerated at these positions either (Figure 2E). Unfortunately, longer CAMSAP3 peptides that included these residues did not yield any well-diffracting crystals; the role of P459 and T460 of CAMSAP3 in katanin binding could thus not be assessed.

To complement the SPOT analysis, we performed SV AUC experiments with CAMSAP3p1 variants with two CAMSAP3p1 double mutants (P459A and I461A, or L465A and I467A). The analysis demonstrates that, as expected, none of the mutants showed any binding to p60N/p80C (Figure 2F). Together, these data demonstrate that a short helical motif of CAMSAP3 binds to the interface formed between the p60N and p80C subunits of katanin through a series of mostly hydrophobic interactions.

CAMSAP3 and ASPM Compete for the Same Binding Site on Katanin

Comparison of the p60N/p80C/CAMSAP3p2 and p60N/p80C/ASPMp complex structures showed that they are very similar. Superimposition revealed no structural changes within the p60N and p80C subunits (Figure 3A): The structures can be superimposed with a root-mean-square deviation of 0.6 Å over all Cα atoms. Strikingly, CAMSAP3p2 and ASPMp share the same binding site on katanin (Figure 3A): I461 of CAMSAP3p2 and F352 of ASPM bind into the same hydrophobic pocket formed by L18 and L19 of p60N and Y574 of p80C (Figures 3A and 3B). Importantly, in both cases, individual mutation of all these hydrophobic residues strongly inhibited or abolished the interactions with the corresponding peptides (Figures 2B and 2F) (Jiang et al., 2017). However, by analyzing the sequences of the CAMSAP3p2 and ASPMp peptides that are necessary for the interaction with p60N/p80C, we were not able to derive any common motif as the sequences are completely different (Figure S2G). Moreover, ASPMp is unfolded in its bound state, whereas CAMSAP3p2 forms a short helix when complexed with p60N/p80C.

The strong overlap between the binding sites of CAMSAP3p2 and ASPMp on katanin suggests that these interactions are mutually exclusive. Indeed, SV AUC experiments revealed that FITC-CAMSAP3p1 and a TAMRA-labeled ASPM peptide (ASPM residues 347–365, denoted TAMRA-ASPMp; Jiang et al., 2017) compete for the same binding site on katanin. In the experiments, we first formed the complexes p60N/p80C/FITC-CAMSAP3p1 (detected at 490 nm) or p60N/p80C/TAMRA-ASPMp (detected at 555 nm) and then added different concentrations of unlabeled ASPMp or CAMSAP3p1, respectively. The experiments showed that once the p60N/p80C/FITC-CAMSAP3p1 complex was preformed, it was difficult to displace FITC-CAMSAP3p1 with ASPMp even when a very high concentration of ASPMp was used (Figure 3C). On the other hand, if the p60N/p80C/TAMRA-ASPMp complex was preformed, TAMRA-ASPMp could be easily displaced by CAMSAP3p1 (Figure 3D). These results suggest that the two peptides indeed compete with each other and that CAMSAP3p1 has a higher affinity for the p60N/p80C heterodimer compared with ASPMp.

Mutation of a Single Katanin Residue Causes Elongation of CAMSAP-Decorated Stretches at Microtubule Minus Ends

Our previous work showed that katanin depletion causes elongation of CAMSAP2-decorated microtubule minus-end stretches, indicating that katanin is a negative regulator of CAMSAP-dependent minus-end stabilization (Jiang et al., 2014). If the interaction between CAMSAPs and katanin is essential for this regulation, mutations disrupting the binding of CAMSAPs to p60N/p80C should have a similar effect on the length of CAMSAP stretches. Previously, we have generated a HeLa cell line, in which a single-residue mutation corresponding to the mouse p80 Y574A (Y571A in human) was introduced into all endogenous copies of the p80-encoding gene using CRISPR/Cas9 technology (Jiang et al., 2017). This mutation disrupted the ASPM-katanin interaction and recapitulated phenotypes of ASPM and katanin loss (Jiang et al., 2017). Since this mutation also inhibits CAMSAP-katanin binding (Figure 2B), we tested its impact on the length of CAMSAP2 stretches in interphase cells, and found that they were strongly elongated (Figures 4A–4C). This effect was identical to that of a complete knockout of p80 (Figures 4A–4C), in spite of the fact that the levels of both p60 and p80 were completely normal in the $p80^{Y571A}$ line (Figure 4A).

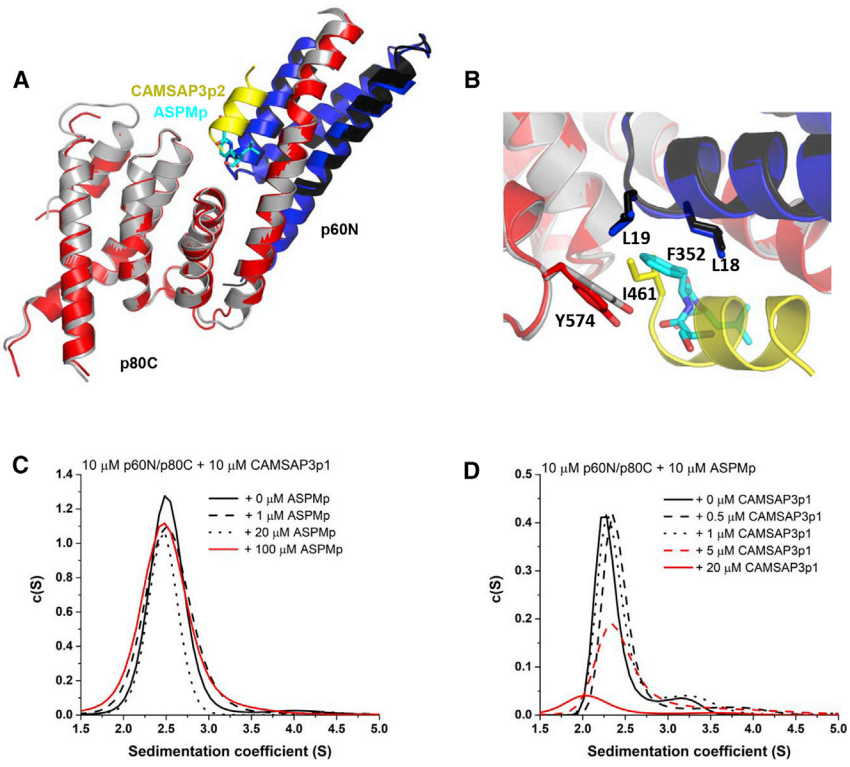

Figure 3. CAMSAP and ASPM Peptides Compete for the Same Binding Site on Katanin

(A) Superimposition of the p60N/p80C/CAMSAP3p2 and p60N/p80C/ASPMp structures. p60N/p80C/CAMSAP3p2: p60N, blue; p80C, red; CAMSAP3p2 peptide, yellow. p60N/p80C/ASPMp: p60N, black; p80C, gray; ASPMp, cyan.

(B) Close-up view of the common CAMSAP3 and ASPM binding site. Interacting residues are shown in stick representation.

(C and D) c(S) distribution profiles of competition assays. (C) Displacement of FITC-CAMSAP3p1 by TAMRA-ASPMp, recorded at 490 nm, which allows the specific detection of the FITC-labeled CAMSAP3p1 peptide. (D) Displacement of TAMRA-ASPMp by FITC-CAMSAP3p1, recorded at 555 nm, which allows specific detection of the TAMRA-labeled ASPMp peptide.

This result supports the view that the CAMSAP-katanin interaction in cells has the same sequence requirements as the one established between CAMSAP3p1 and the p60N/p80C heterodimer *in vitro*. It further demonstrates the importance of CAMSAP-katanin complex formation for the proper regulation of the length of CAMSAP-decorated stretches at microtubule minus ends.

DISCUSSION

In this study, we have determined the structural basis of the interaction between a peptide of CAMSAP3 and the katanin p60/p80 heterodimer. The p60N/p80C/CAMSAPp2 structure shares remarkable similarity to that of the p60N/p80C/ASPMp complex, as both the CAMSAP3p2 and ASPMp peptides bind to the same site formed at the interface between the p60N and p80C subunits. Therefore, the same set of katanin residues is involved in the interaction with both partners, and thus the point mutations in p60 and p80, which specifically disrupt the ASPM-katanin complex, also abolish the CAMSAP-katanin interaction. For example, a point mutation in a conserved tyrosine residue in p80 (Y574 in mouse and Y571 in human), which we previously showed to prevent ASPM-katanin binding and affect spindle flux and spindle positioning (Jiang et al., 2017), also blocked CAMSAP binding and thus caused elongation of CAMSAP2-decorated microtubule stretches, similar to a complete katanin knockout. A microcephaly-associated mutation in p80, S538L, also inhibited CAMSAP binding, thus suggesting that not only mitotic spindles but also interphase microtubule arrays may be affected in microcephaly patients with mutations in the p80-encoding gene.

Although ASPM and CAMSAP2/3 use the same binding site on katanin, their katanin-binding sequences share no apparent similarity, apart from both being involved in establishing hydrophobic contacts with the p60/p80 heterodimer. While an unfolded peptide is responsible for ASPM binding to katanin, a short helix performs this role in CAMSAP3. In our *in vitro* assays, the CAMSAP3 peptide displayed a higher affinity for the p60N/p80C heterodimer, which is consistent with the fact that more contacts between the CAMSAP3 peptide and katanin p60N/p80C heterodimer were observed in the complex structure. However, the affinity of the full-length ASPM for katanin might not necessarily be lower, because the katanin-binding peptide is repeated in ASPM three times, and the mutation of two of the three repeats strongly inhibited the katanin-ASPM interaction (Jiang et al., 2017). This observation indicates that several ASPM repeats contribute to the binding mechanism. Furthermore, in cells, ASPM and CAMSAP2/3 do not compete for binding to katanin on microtubules, because ASPM is sequestered in the nucleus during interphase, while CAMSAP2 and CAMSAP3 dissociate from microtubules in mitosis (Jiang et al., 2014; Syred et al., 2013).

Our *in vitro* reconstitution assays showed that ASPM and katanin can cooperatively regulate the stability of both microtubule lattices and minus ends: ASPM can promote both the loading of katanin onto microtubules as well as their severing. Furthermore, the two proteins can act together to block minus-end elongation (Jiang et al., 2017). The latter effect depends on the autonomous recognition of microtubule minus ends by ASPM and also on the end-binding properties of the p60N/p80C heterodimer. It is possible that the CAMSAP2/3-katanin complex would modulate interphase microtubule minus ends in a similar way: It could cause severing of CAMSAP-decorated stretches thus affecting their number and lifetime and also limit their formation by blocking microtubule extension from the minus end. The interaction between CAMSAPs and katanin might also potentially promote CAMSAP recruitment to microtubule minus ends generated by katanin-mediated severing, for example, when such ends are released from the centrosome (Jiang et al., 2014; Wang et al., 2017).

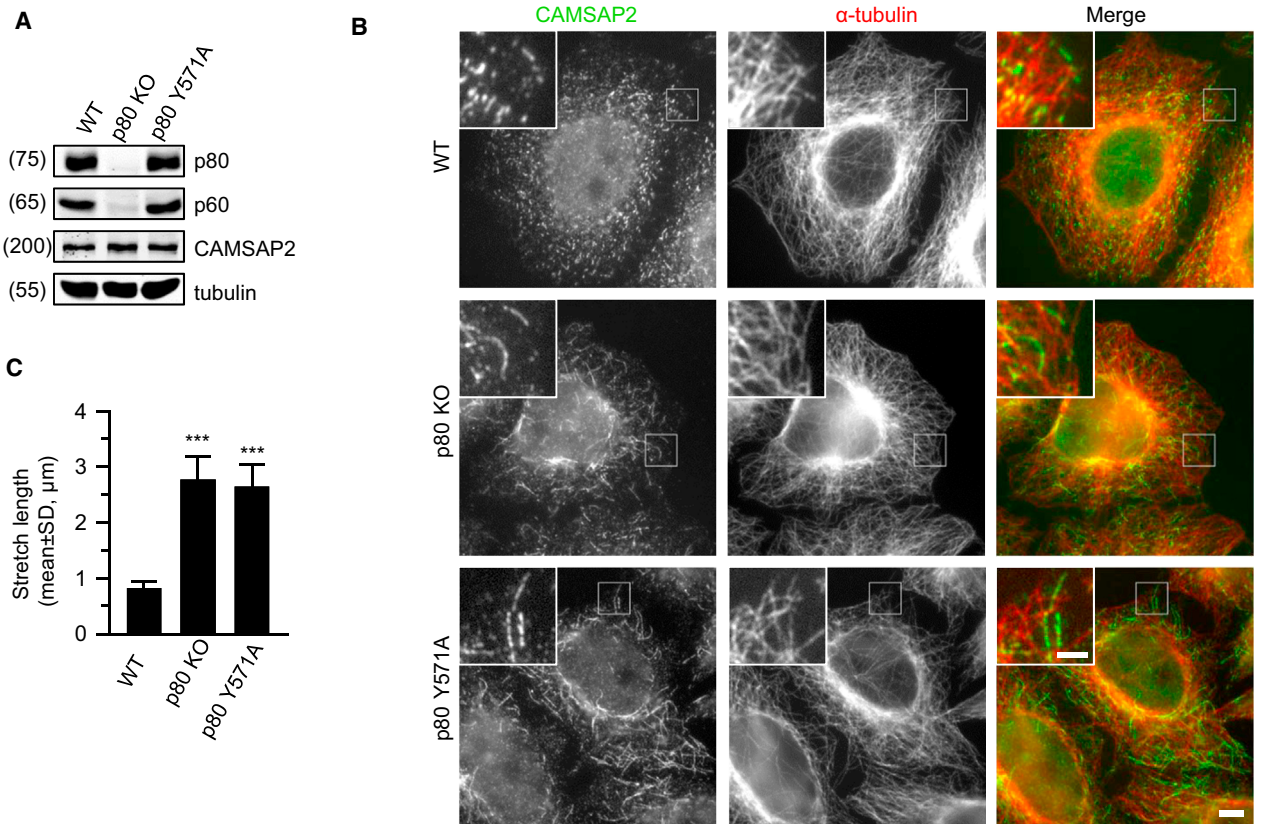

Figure 4. The CAMSAP-Katanin Interaction Is Required to Restrict the Length of CAMSAP-Decorated Microtubule Stretches

(A) Western blots with the indicated antibodies of extracts of wild-type (WT), p80 knockout (KO) and p80Y571A HeLa cells. Katanin protein levels in WT and p80Y571A mutant cell lines are similar.

(B) Immunostaining for α-tubulin (red) and CAMSAP2 (green) in WT, p80 KO, and p80Y571A HeLa cells. Scale bar, 5 μm; inset, 2 μm.

(C) Quantification of CAMSAP2-decorated microtubule stretch length for the experiments shown in (B). CAMSAP2-decorated stretches in 20 cells were measured per condition. Data represent mean ± SD. ***$p < 0.001$, Mann-Whitney U test.

The microtubule minus-end regulating katanin-CAMSAP complex described here is likely to be evolutionarily conserved, as fly katanin together with the spectraplakin Short stop can form a complex with the CAMSAP homolog Patronin in *Drosophila* embryos (Drozdetskiy et al., 2015). Together, these proteins form cortical, non-centrosomal microtubule-organizing centers, but the exact role of katanin in these structures still needs to be investigated. Also in mammalian epithelial cells, CAMSAP3 cooperates with the spectraplakin ACF7 to stabilize non-centrosomal microtubule arrays at the cell cortex (Ning et al., 2016; Noordstra et al., 2016), and it will be interesting to assess whether katanin also plays a role in this process. Toward this aim, our structural work provides a basis to explore the mechanism underlying the cross-talk between CAMSAPs and katanin in microtubule minus-end organization in different systems.

STAR★METHODS

Detailed methods are provided in the online version of this paper and include the following:

- KEY RESOURCES TABLE
- CONTACT FOR REAGENT AND RESOURCE SHARING
- EXPERIMENTAL MODEL AND SUBJECT DETAILS
- METHOD DETAILS
  - DNA Constructs, Cell Transfection and Pull Down Assays
  - Protein Expression and Purification
  - Analytical Ultracentrifugation
  - Circular Dichroism Spectroscopy
  - Synthetic Peptide Arrays on Cellulose Membranes (SPOT)
  - Crystallization and Structure Determination
  - Antibodies and Immunofluorescence Cell Staining
  - Imaging and Image Preparation for Publication
- QUANTIFICATION AND STATISTICAL ANALYSIS
- DATA AND SOFTWARE AVAILABILITY

SUPPLEMENTAL INFORMATION

Supplemental Information includes three figures and can be found with this article online at https://doi.org/10.1016/j.str.2017.12.017.

ACKNOWLEDGMENTS

We thank the beamline scientists at beamlines X06DA of the Swiss Light Source (Paul Scherrer Institut, Villigen, Switzerland) for technical assistance

with the X-ray data collection. This work was supported by the Netherlands Organization for Scientific Research ALW Open Program grant 824.15.017 to A.A., the EMBO long-term and Marie Curie IEF fellowships to L.F. (awarded under maiden name L. Rezabkova), and grants from the Swiss National Science Foundation (31003A_166608 to M.O.S. and 31003A_163449 to R.A.K.).

AUTHOR CONTRIBUTIONS

K.J., L.F., S.H., G.C., R.A.K., M.O.S., R.V., and A.A. designed experiments, analyzed the data, and wrote the paper. A.A. coordinated the project and supervised cell biological experiments and pull-down assays. M.O.S. supervised the X-ray crystallography experiments. R.A.K. supervised the biophysical experiments. R.V. supervised the SPOT experiments. K.J. and S.H. performed pull-down assays and cell biological experiments, L.F. performed biophysical experiments, L.F., G.C., and A.E.P. performed crystallography experiments and solved the structure, and C.L. performed SPOT experiments.

DECLARATION OF INTERESTS

The authors declare no competing financial interests.

Received: September 12, 2017
Revised: November 28, 2017
Accepted: December 28, 2017
Published: January 25, 2018

REFERENCES

Adams, P.D., Afonine, P.V., Bunkoczi, G., Chen, V.B., Davis, I.W., Echols, N., Headd, J.J., Hung, L.W., Kapral, G.J., Grosse-Kunstleve, R.W., et al. (2010). PHENIX: a comprehensive Python-based system for macromolecular structure solution. Acta Crystallogr. D Biol. Crystallogr. *66*, 213–221.

Akhmanova, A., and Hoogenraad, C.C. (2015). Microtubule minus-end-targeting proteins. Curr. Biol. *25*, R162–R171.

Akhmanova, A., and Steinmetz, M.O. (2015). Control of microtubule organization and dynamics: two ends in the limelight. Nat. Rev. Mol. Cell Biol. *16*, 711–726.

Atherton, J., Jiang, K., Stangier, M.M., Luo, Y., Hua, S., Houben, K., van Hooff, J.J.E., Joseph, A.P., Scarabelli, G., Grant, B.J., et al. (2017). A structural model for microtubule minus-end recognition and protection by CAMSAP proteins. Nat. Struct. Mol. Biol. *24*, 931–943.

Baines, A.J., Bignone, P.A., King, M.D., Maggs, A.M., Bennett, P.M., Pinder, J.C., and Phillips, G.W. (2009). The CKK domain (DUF1781) binds microtubules and defines the CAMSAP/ssp4 family of animal proteins. Mol. Biol. Evol. *26*, 2005–2014.

Bond, J., Roberts, E., Mochida, G.H., Hampshire, D.J., Scott, S., Askham, J.M., Springell, K., Mahadevan, M., Crow, Y.J., Markham, A.F., et al. (2002). ASPM is a major determinant of cerebral cortical size. Nat. Genet. *32*, 316–320.

Buey, R.M., Sen, I., Kortt, O., Mohan, R., Gfeller, D., Veprintsev, D., Kretzschmar, I., Scheuermann, J., Neri, D., Zoete, V., et al. (2012). Sequence determinants of a microtubule tip localization signal (MtLS). J. Biol. Chem. *287*, 28227–28242.

Dammermann, A., Desai, A., and Oegema, K. (2003). The minus end in sight. Curr. Biol. *13*, R614–R624.

Davis, I.W., Murray, L.W., Richardson, J.S., and Richardson, D.C. (2004). MOLPROBITY: structure validation and all-atom contact analysis for nucleic acids and their complexes. Nucleic Acids Res. *32*, W615–W619.

Drozdetskiy, A., Cole, C., Procter, J., and Barton, G.J. (2015). JPred4: a protein secondary structure prediction server. Nucleic Acids Res. *43*, W389–W394.

Emsley, P., Lohkamp, B., Scott, W.G., and Cowtan, K. (2010). Features and development of COOT. Acta Crystallogr. D Biol. Crystallogr. *66*, 486–501.

Goodwin, S.S., and Vale, R.D. (2010). Patronin regulates the microtubule network by protecting microtubule minus ends. Cell *143*, 263–274.

Hartman, J.J., Mahr, J., McNally, K., Okawa, K., Iwamatsu, A., Thomas, S., Cheesman, S., Heuser, J., Vale, R.D., and McNally, F.J. (1998). Katanin, a microtubule-severing protein, is a novel AAA ATPase that targets to the centrosome using a WD40-containing subunit. Cell *93*, 277–287.

Hu, W.F., Pomp, O., Ben-Omran, T., Kodani, A., Henke, K., Mochida, G.H., Yu, T.W., Woodworth, M.B., Bonnard, C., Raj, G.S., et al. (2014). Katanin p80 regulates human cortical development by limiting centriole and cilia number. Neuron *84*, 1240–1257.

Jiang, K., Hua, S., Mohan, R., Grigoriev, I., Yau, K.W., Liu, Q., Katrukha, E.A., Altelaar, A.F., Heck, A.J., Hoogenraad, C.C., and Akhmanova, A. (2014). Microtubule minus-end stabilization by polymerization-driven CAMSAP deposition. Dev. Cell *28*, 295–309.

Jiang, K., Toedt, G., Montenegro Gouveia, S., Davey, N.E., Hua, S., van der Vaart, B., Grigoriev, I., Larsen, J., Pedersen, L.B., Bezstarosti, K., et al. (2012). A Proteome-wide screen for mammalian SxIP motif-containing microtubule plus-end tracking proteins. Curr. Biol. *22*, 1800–1807.

Jiang, K., Rezabkova, L., Hua, S., Liu, Q., Capitani, G., Altelaar, A.F.M., Heck, A.J.R., Kammerer, R.A., Steinmetz, M.O., and Akhmanova, A. (2017). Microtubule minus-end regulation at spindle poles by an ASPM/katanin complex. Nat. Cell Biol. *19*, 480–492.

Kabsch, W. (2010). XDS. Acta Crystallogr. D Biol. Crystallogr. *66*, 125–132.

McNally, F.J., and Vale, R.D. (1993). Identification of katanin, an ATPase that severs and disassembles stable microtubules. Cell *75*, 419–429.

Meng, W., Mushika, Y., Ichii, T., and Takeichi, M. (2008). Anchorage of microtubule minus ends to adherens junctions regulates epithelial cell-cell contacts. Cell *135*, 948–959.

Mishra-Gorur, K., Çağlayan, A.O., Schaffer, A.E., Chabu, C., Henegariu, O., Vonhoff, F., Akgümüş, G.T., Nishimura, S., Han, W., Tu, S., et al. (2014). Mutations in KATNB1 cause complex cerebral malformations by disrupting asymmetrically dividing neural progenitors. Neuron *84*, 1226–1239.

Mochida, G.H., and Walsh, C.A. (2001). Molecular genetics of human microcephaly. Curr. Opin. Neurol. *14*, 151–156.

Ning, W., Yu, Y., Xu, H., Liu, X., Wang, D., Wang, J., Wang, Y., and Meng, W. (2016). The CAMSAP3-ACF7 complex couples noncentrosomal microtubules with actin filaments to coordinate their dynamics. Dev. Cell *39*, 61–74.

Noordstra, I., Liu, Q., Nijenhuis, W., Hua, S., Jiang, K., Baars, M., Remmelzwaal, S., Martin, M., Kapitein, L.C., and Akhmanova, A. (2016). Control of apico-basal epithelial polarity by the microtubule minus-end-binding protein CAMSAP3 and spectraplakin ACF7. J. Cell Sci. *129*, 4278–4288.

Rezabkova, L., Jiang, K., Capitani, G., Prota, A.E., Akhmanova, A., Steinmetz, M.O., and Kammerer, R.A. (2017). Structural basis of katanin p60:p80 complex formation. Sci. Rep. *7*, 14893.

Roll-Mecak, A., and McNally, F.J. (2010). Microtubule-severing enzymes. Curr. Opin. Cell Biol. *22*, 96–103.

Schuck, P. (2000). Size-distribution analysis of macromolecules by sedimentation velocity ultracentrifugation and lamm equation modeling. Biophys. J. *78*, 1606–1619.

Syred, H.M., Welburn, J., Rappsilber, J., and Ohkura, H. (2013). Cell cycle regulation of microtubule interactomes: multi-layered regulation is critical for the interphase/mitosis transition. Mol. Cell. Proteomics *12*, 3135–3147.

Wang, J., Xu, H., Jiang, Y., Takahashi, M., Takeichi, M., and Meng, W. (2017). CAMSAP3-dependent microtubule dynamics regulates Golgi assembly in epithelial cells. J. Genet. Genomics *44*, 39–49.

Wenschuh, H., Volkmer-Engert, R., Schmidt, M., Schulz, M., Schneider-Mergener, J., and Reineke, U. (2000). Coherent membrane supports for parallel microsynthesis and screening of bioactive peptides. Biopolymers *55*, 188–206.

Zheng, J., Furness, D., Duan, C., Miller, K.K., Edge, R.M., Chen, J., Homma, K., Hackney, C.M., Dallos, P., and Cheatham, M.A. (2013). Marshalin, a microtubule minus-end binding protein, regulates cytoskeletal structure in the organ of Corti. Biol. Open *2*, 1192–1202.

STAR★METHODS

KEY RESOURCES TABLE

REAGENT or RESOURCE	SOURCE	IDENTIFIER
Antibodies		
GFP	Abcam	Cat# ab290; RRID: AB_303395
katanin p60	Proteintech	Cat# 17560-1-AP; RRID: AB_10694670
katanin p80	Proteintech	Cat# 14969-1-AP; RRID: AB_10637861
CAMSAP2	Novus	Cat# NBP1-21402; RRID: AB_1659977
α-tubulin	Pierce	Cat# MA1-80017; RRID: AB_2210201
β-tubulin	Sigma-Aldrich	Cat# T5201; RRID: AB_609915
Bacterial and Virus Strains		
E.Coli BL21 (DE3)	Agilent	200131
Chemicals, Peptides, and Recombinant Proteins		
Dynabeads M-280 Streptavidin	ThermoFisher	11206D
StrepTactin Sepharose High Performance	GE Healthcare	28-9355-99
Polyethylenimine	Polysciences	24765-2
cOmplete™ Protease Inhibitor Cocktail	Roche	4693116001
HisTrap FF, 5 ml column	GE Healthcare	17-5255-01
HiLoad 16/600 Superdex 75 pg column	GE Healthcare	28-9893-33
CAMSAP3p1 - assembled on synthesizer	This paper	N/A
CAMSAP3p2 – assembled on synthesizer	This paper	N/A
CAMSAP3p1 P495A, I461A - assembled on synthesizer	This paper	N/A
CAMSAP3p1 L465A, I467A - assembled on synthesizer	This paper	N/A
ASPMp - assembled on synthesizer	Jiang et al., 2017	N/A
GST-p80C/p60N	Jiang et al., 2017	N/A
p80C/p60N	Jiang et al., 2017	N/A
p80C/p60N M501A	This paper	N/A
Deposited Data		
Atomic coordinates and structure factors	PDBe	5OW5
Western blotting and cell biology data	Mendeley Data	https://doi.org/10.17632/73f8dzrvfj.2
Biophysical measurements data	Mendeley Data	https://doi.org/10.17632/78676pyggn.2
Experimental Models: Cell Lines		
Human: HEK293T	ATCC	CRL-11268
Human: HeLa	ATCC	CCL-2.2
Human: HeLa katanin p80 Y571A	Jiang et al., 2017	
Recombinant DNA		
Bio-GFP-CAMSAP3 full length	Jiang et al., 2014	N/A
Bio-GFP-CAMSAP3 N1	This paper	N/A
Bio-GFP-CAMSAP3 N2	This paper	N/A
Bio-GFP-CAMSAP3 C1	This paper	N/A
Bio-GFP-CAMSAP3 C2	This paper	N/A
Bio-GFP-CAMSAP3p1	This paper	N/A
Strep-GFP-CAMSAP3p1	This paper	N/A
Strep-GFP-CAMSAP3 456-520	This paper	N/A
GST-CAMSAP3p1	This paper	N/A
GFP-katanin p60	Jiang et al., 2017	N/A
GFP-katanin p60N	This paper	N/A

(*Continued on next page*)

Continued

REAGENT or RESOURCE	SOURCE	IDENTIFIER
GFP-katanin p60 L18A		
GFP-katanin p60 L19A	Jiang et al., 2017	N/A
GFP-katanin p80	Jiang et al., 2017	N/A
GFP-katanin p80C	Jiang et al., 2017	N/A
GFP-katanin p80 M501A	This paper	N/A
GFP-katanin p80 Y574A	Jiang et al., 2017	N/A
GFP-katanin p80 S538L	Jiang et al., 2017	N/A
Software and Algorithms		
Sigmaplot 12	Systat Software Inc	https://systatsoftware.com/
Jpred 4	Drozdetskiy et al., 2015	http://www.compbio.dundee.ac.uk/jpred/
ImageJ	NIH	https://imagej.nih.gov/ij/
OriginPro 2016	OriginLab	www.OriginLab.com
Sedfit	Schuck, 2000	https://sedfitsedphat.nibib.nih.gov/software/default.aspx
XDS	Kabsch, 2010	http://xds.mpimf-heidelberg.mpg.de
Phenix	Adams et al., 2010	https://www.phenix-online.org/documentation/reference/refinement.html
COOT	Emsley et al., 2010	https://www2.mrc-lmb.cam.ac.uk/personal/pemsley/coot/

CONTACT FOR REAGENT AND RESOURCE SHARING

Further information and requests for resources and reagents should be directed to and will be fulfilled by the Lead Contact, Anna Akhmanova (a.akhmanova@uu.nl).

EXPERIMENTAL MODEL AND SUBJECT DETAILS

We used *E.coli* BL21 (DE3) cells for recombinant expression of p60N/p80C for biochemical, biophysical and X-ray crystallography experiments. The cells were cultured standardly in LB media.

We used HEK293T and HeLa cell lines, which are not listed in the database of commonly misidentified cell lines maintained by ICLAC and NCBI BioSample. Katanin p80 knock out and *p80*^{Y571A} mutant (Y574A in mouse) cell lines in HeLa were described previously (Jiang et al., 2017). Cells were negative for mycoplasma contamination. Cell lines were cultured in DMEM/F10 (1:1) supplemented with 10% FBS and 5 U/ml penicillin and 50 μg/ml streptomycin.

METHOD DETAILS

DNA Constructs, Cell Transfection and Pull Down Assays

Bio-GFP-CAMSAP3 full length was described previously (Jiang et al., 2014). A substrate peptide for the biotin ligase BirA (Bio-tag, MASGLNDIFEAQKIEWHE) was inserted at the N-terminus of GFP-tagged bait proteins. Biotinylation was accomplished by co-expressing the tagged proteins together with BirA. CAMSAP3 deletion mutants were generated by using PCR-based strategies. All katanin constructs were described previously (Jiang et al., 2017), except the katanin p80 M501A mutant, which was generated by a Gibson Assembly-based approach.

Polyethylenimine (PEI, Polysciences) was used to transfect HEK293T cells for GST and streptavidin pull down experiments. GST and streptavidin pull down assays with extracts of transfected HEK293T cells were carried out as described previously (Jiang et al., 2012). Briefly, transfected cells were lysed in the lysis buffer I (50 mM HEPES, 150 mM NaCl and 0.5% Triton X-100, pH 7.4) supplemented with protease inhibitors (Roche). After spinning down the debris, the supernatant were incubated with beads for 45 min, followed by three washing steps in the wash buffer (50 mM HEPES, 150 mM NaCl and 0.1% Triton X-100, pH 7.4). The bait and the bound proteins were eluted in SDS-PAGE sample buffer by boiling for 5 min.

Protein Expression and Purification

The p60N/p80C complex was cloned, co-expressed and purified as described previously (Jiang et al., 2017). GST-CAMSAP3p1 was expressed in *E.coli* and coupled to Glutathione Sepharose 4 Fast Flow resin (GE Healthcare, Lifescience) following the standard protocol from the vendor. All p60N/p80C mutants were generated using the QuickChange approach. CAMSAP3 and FITC-labelled CAMSAP3 peptides were assembled on an automated continuous-flow synthesizer employing standard methods.

To purify strep-GFP-CAMSAP3 fragments, 36 h post transfection, HEK293T cells from two 15 cm dishes were lysed in 1.8 ml lysis buffer II (50 mM HEPES, 300 mM NaCl and 0.5% Triton X-100, pH 7.4) supplemented with protease inhibitors (Roche). After spinning down the debris, the supernatant were incubated with 160 μl beads for 45 min. Beads were washed five times in the lysis buffer II without protease inhibitors and twice with the wash buffer II (50 mM HEPES, 150 mM NaCl and 0.01% Triton X-100, pH 7.4). The proteins were eluted in 100 μl elution buffer (50 mM HEPES, 150 mM NaCl, 0.01% Triton X-100 and 2.5 mM desthiobiotin, pH 7.4), snap frozen in liquid nitrogen and stored in -80°C.

Analytical Ultracentrifugation

Sedimentation velocity experiments were performed using a ProteomeLab XL-I Beckman Coulter analytical ultracentrifuge equipped with an AN50Ti rotor. All measurements were conducted at 20 °C and at 42 000 rpm in 20 mM HEPES, pH 7.5, supplemented with 150 mM NaCl and 2 mM 2-mercaptoethanol. All data were collected at 280, 490 or 555 nm using an absorbance optical system. Data analysis was performed with the SEDFIT package (Schuck, 2000) using a sedimentation coefficient distribution model c(s). Detection of the FITC-labelled CAMSAP3 peptide (AA 456-470, denoted FITC-CAMSAP3p1) was carried out with excitation at 490 nm, detection of TAMRA-labelled ASPM peptide (residues 347-365, denoted TAMRA-ASPMp) with excitation at 555 nm.

Circular Dichroism Spectroscopy

Far-ultra violet circular dichroism spectra of wild-type and mutant p60N/p80C complexes (5 μM) were obtained by scanning wavelengths from 200 nm to 260 nm using a Chirascan-Plus instrument (Applied Photophysics Ltd.) equipped with a computer-controlled Peltier element. All experiments were performed in PBS. A ramping rate of 1 °C per min was used to record thermal unfolding profiles. Midpoints of the transitions, T_m, were taken as the maximum of the derivative $d[\theta]_{222}/dT$.

Synthetic Peptide Arrays on Cellulose Membranes (SPOT)

Cellulose membrane-bound peptide arrays were prepared according to standard SPOT synthesis protocols using a SPOT synthesizer as described in detail (Wenschuh et al., 2000). The experiments were done as described in (Buey et al., 2012). Arrays were probed with a solution of His6 p60N/p80C at a concentration of 100 μg/ml.

Crystallization and Structure Determination

Protein complexes in 20 mM HEPES, pH 7.5, supplemented with 150 mM NaCl were concentrated to 20 mg/ml prior to crystallization. For obtaining good quality crystals different lengths of the CAMSAP3 peptide were screened. Crystals of the p60N/p80C/CAMSAP3p2 peptide (AA 461-470) complex grew within a few hours at 20°C using the sitting drop method in 20% PEG 3350, 0.1 M BisTris propane (5.5), 0.2 M NaF. For cryo-protection, the reservoir solution was supplemented with 20% ethylene-glycol. Native data were acquired at the X06DA beamline of the Swiss Light Source to a resolution of 1.7 Å. Data were integrated and scaled using XDS (Kabsch, 2010). The structure was solved by molecular replacement in space group $P2_1$ using the p60N/p80C chains of the p60N/p80C/ASPMp complex (PDB: 5LB7) (Jiang et al., 2017) as a search model. Structure refinement was carried out with Phenix.refine from the Phenix suite (Adams et al., 2010). The program COOT was used for manual real space refinement (Emsley et al., 2010). Data and refinement statistics are reported in Table 1.

Antibodies and Immunofluorescence Cell Staining

We used rabbit polyclonal antibodies against katanin p60 and p80 (Proteintech, 17560-1-AP and 14969-1-AP), CAMSAP2 (Novus, NBP1-21402), GFP (Abcam, ab290), and a rat monoclonal antibody against α-tubulin YL1/2 (Pierce, MA1-80017). To co-label microtubules and CAMSAP2, cells were fixed with –20°C methanol for 10 min. Cells were rinsed with 0.15% Triton X-100 in PBS; subsequent washing and labeling steps were carried out in PBS supplemented with 2% bovine serum albumin and 0.05% Tween-20. At the end, slides were rinsed in 70% and 100% ethanol, air-dried and mounted in Vectashield mounting medium (Vector laboratories).

Imaging and Image Preparation for Publication

Cell images were collected with a Nikon Eclipse 80i equipped with a Plan Apo VC 100x 1.4 N.A. oil objectives and a CoolSNAP HQ2 camera (Roper Scientific). Images were prepared for publication using Adobe Photoshop. All images were modified by adjustments of levels and contrast.

QUANTIFICATION AND STATISTICAL ANALYSIS

The binding curve describing the interaction between FITC-CAMSAP3p1and p60N/p80C complex was generated as described previously (Jiang et al., 2017). Shortly, the c(s) distribution of the p60N/p80C complex was integrated and the fraction of FITC-CAMSAP3p1peptide bound (FB) was calculated from the equation:

$$FB = (A_{obs}-A_{min})/(A_{max}-A_{min})$$

where A_{max} is the maximum area under the peak at saturating p60N/p80C protein complex concentrations, A_{obs} is the area under the peak for any p60N/p80C concentration, and A_{min} corresponds to the area under the peak in the absence of p60N/p80C. FB was

plotted against the p60N/p80C protein concentration. The equilibrium dissociation constant, K_d, of the p60N/p80C/CAMSAP3p1 complex was obtained by fitting the data to the equation

$$FB = \left\{ Kd + P1 + P2 - \sqrt{(Kd + P1 + P2)^2 - 4P1P2} \right\} \Big/ 2$$

where P1 is the concentration of FITC-CAMSAP3p1 and P2 is the concentration of the p60N/p80C complex. All fittings were performed using the ORIGIN software package.

Data on the length of CAMSAP2-decorated stretches were collected in 2 independent experiments. 20 cells were measured per condition. Quantifications were performed in ImageJ. Data represent mean ± SD. Statistical analysis using Mann-Whitney U test was performed in SigmaPlot.

DATA AND SOFTWARE AVAILABILITY

The atomic coordinates and structure factors of the p60N/p80C/CAMSAP3p2 complex have been deposited to the RCSB PDB (www.rcsb.org) with the PDB ID 5OW5. The unproccesed Western blot and cell biology data were deposited at https://data.mendeley.com/ under https://doi.org/10.17632/73f8dzrvfj.2 and the data on biophysical measurements under https://doi.org/10.17632/78676pyggn.2.